Theory and practice of the FFT/matrix inversion technique for probe-corrected spherical near-field antenna measurements with high-order probes

Laitinen, Tommi; Pivnenko, Sergey; Nielsen, Jeppe Majlund; Breinbjerg, Olav

Published in:
I E E E Transactions on Antennas and Propagation

Link to article, DOI:
10.1109/TAP.2010.2050437

Publication date:
2010

Document Version
Publisher's PDF, also known as Version of record

Theory and Practice of the FFT/Matrix Inversion Technique for Probe-Corrected Spherical Near-Field Antenna Measurements With High-Order Probes

Tommi Laitinen, *Member, IEEE*, Sergey Pivnenko, *Member, IEEE*, Jeppe Majlund Nielsen, and Olav Breinbjerg, *Member, IEEE*

***Abstract*—A complete antenna pattern characterization procedure for spherical near-field antenna measurements employing a high-order probe and a full probe correction is described. The procedure allows an (almost) arbitrary antenna to be used as a probe. Different measurement steps of the procedure and the associated data processing are described in detail, and comparison to the existing procedure employing a first-order probe is made. The procedure is validated through measurements.**

***Index Terms*—Antenna measurements, high-order probe, near-field scanning, probe correction, spherical wave expansion.**

I. Introduction

THE Technical University of Denmark (DTU) and the European Space Agency (ESA) have a 30-year history of accurate probe-corrected spherical near-field antenna measurements at the DTU-ESA Spherical Near-Field Antenna Test Facility [1]. The standard procedure for the antenna pattern characterization applied at the DTU-ESA Facility is based on the use of so-called first-order ($|\mu| = 1$) probes, since they can exploit the computationally efficient and stable first-order probe correction technique [2]. These probes are conical horns fed by circular waveguides excited with the dominant mode. The conical horn probes are typically operated on a relatively narrow frequency band, about 10%–15%, thus the collection of probes at the DTU-ESA Facility consists of 14 dual-polarized probes to cover the frequency range from 3–18 GHz. This type of a probe also becomes relatively heavy and large at low frequencies, for example, below 3 GHz.

The capacity of computers has increased significantly during the latest 30 years. For this reason, the computational efficiency of the probe correction has become a less significant factor for many applications, whereas it has become attractive to consider, also at the expense of reduced computational efficiency, such probe correction techniques that would be applicable for high-order ($|\mu| > 1$) probes, or, more generally, for probes that are not of the first order. In this paper, we understand high-order probes generally as those not belonging to the class of first-order probes. The use of a high-order probe correction technique allows a greater flexibility in choosing a probe that leads to an optimal compromise between the desired properties of the probe, for example, the bandwidth, the weight, the size, and the cost.

In fact, several high-order probe correction techniques have been introduced recently [3]–[10]. Some of these techniques are based on the spherical wave expansion of the AUT and probe fields and involve spherical wave translations in the transmission formula [3]–[6], [8], [9]. As opposed to these, the techniques [7], [10] are based on another type of an expansion involving a plane-wave translation operator in the transmission formula. Among the techniques referred here, the techniques [5], [7], [9] and [10] are the only ones applicable for (almost) arbitrary probes. The work in [5] was carried out during 2004–2006 within a project supported by the European Space Agency [5]. The techniques [7] and [10] were published in 2008 and 2009, respectively.

It has been shown in [7] and [10], that the use of an iterative solver makes it possible to solve the transmission formula in a computationally efficient manner. For example, compared to the direct matrix inversion, the use of the iterative solver has been shown to decrease the computational complexity in solving the transmission formula from $O(N^6)$ to $O(N^4)$ in [7] and further to $O(N^2 \log N)$ in [10]. Here N is proportional to the electrical radius of AUT (antenna under test) minimum sphere. For comparison, the computational complexities of the techniques [5] and [9] are both $O(N^4)$. By noting that the computational complexity of $O(N^4)$ is low enough for a major part of spherical near-field antenna measurement applications, the general high-order probe correction technique presented in [5], that will be referred to as the FFT/matrix inversion technique in this paper, is taken into further consideration here. It is further noted that the technique in [9] is a modification of the FFT/matrix inversion technique applicable in conjunction with another scanning technique.

Naturally, the computation of the far field from the probe signals measured in the near field, including the probe correction, is only one part of a complete antenna pattern characterization procedure. The high-order probe correction techniques presented in the literature so far have, however, not touched upon the practical implementation aspects of the technique for an existing range at all, or have done that in a limited fashion, and for this reason this issue deserves further attention.

Manuscript August 14, 2009; revised January 22, 2010; accepted February 12, 2010. Date of publication May 18, 2010; date of current version August 05, 2010. This work was supported by the ESA/ESTEC under Contract 18222/04/NL/LvH/bj. The work of T. Laitinen was supported by the Academy of Finland (decision notification no. 129055).

T. Laitinen is with the Department of Radio Science and Engineering, Aalto University, FI-00076 Aalto, Finland (e-mail: tommi.laitinen@tkk.fi).

S. Pivnenko, J. M. Nielsen and O. Breinbjerg are with the Technical University of Denmark, Kgs. Lyngby, Denmark (e-mail: sp@elektro.dtu.dk; jmn@elektro.dtu.dk; ob@elektro.dtu.dk).

Digital Object Identifier 10.1109/TAP.2010.2050437

The purpose of this paper is to present the complete antenna pattern characterization procedure developed at the DTU-ESA Facility based on the FFT/matrix inversion technique and employing high-order probes and to describe all practical steps of the procedure with the associated data processing. Comparison to the existing procedure employing first-order probes is made where relevant. The procedure is presented primarily for dual-port probes, but clarifications are provided for the case of a single-port probe. In addition to the earlier validation measurements carried out for 2.9 GHz and 3.0 GHz [5] and reported in [11], another set of validation measurements is carried out here for 1.4 GHz and 1.5 GHz, and the results are presented.

The developed procedure has been tested and shown to work earlier in [5] with computer calculations for the frequency range 1–3 GHz for AUTs with the radius of the minimum sphere up to 3 m, which corresponds to approximately 30 wavelengths. The calculation results have been partly presented in [12], and are thus left outside of this paper.

The theoretical background is presented in Section II. The antenna pattern characterization procedure for high-order probes is described in Section III. Test measurements for validation of the procedure are then presented in Section IV. Conclusions are given in Section V.

II. Background Theory

The theory of probe-corrected spherical near-field antenna measurements with a first-order probe is presented in [2]. The part of this theory relevant to high-order probes is summarized in this section.

A. Measurement Geometry

The geometry for probe-corrected spherical near-field antenna measurements is presented in Fig. 1 where the AUT and the probe minimum spheres are illustrated. The $(x,\ y,\ z)$ and $(x',\ y',\ z')$ and the Cartesian coordinates of the AUT and the probe coordinate systems, respectively. The (r,θ,ϕ) are the standard spherical coordinates of the AUT coordinate system [13]. The measurement distance r is the distance between the origins of the AUT and probe coordinate systems. The χ angle is the probe rotation angle; for $\chi = 0°$ and $\chi = 90°$, the x' axis is parallel to the θ and ϕ unit vectors of the AUT coordinate system, respectively.

B. Spherical Wave Expansion

According to [2], the radiated fields of the AUT and the probe are both expressed in terms of the spherical vector wave expansion (SWE). Assuming and suppressing the time convention of $e^{-i\omega t}$, the practical, truncated form of the SWE of the radiated electric field of the AUT, $\boldsymbol{E}_{AUT}(r,\theta,\phi)$, becomes

$$\boldsymbol{E}_{AUT}(r,\theta,\phi) = \frac{k}{\sqrt{\eta}} \sum_{smn} Q_{smn} \boldsymbol{F}^{(3)}_{smn}(r,\theta,\phi) \qquad (1)$$

where k is the wave number, η is the intrinsic admittance of the ambient medium, Q_{smn} are the spherical vector wave coefficients (Q coefficients) of the AUT field, and $\boldsymbol{F}^{(3)}_{smn}(r,\theta,\phi)$ are the power-normalized spherical vector wave functions [2, Ch. 2]. The triple summation is for $m = -M \ldots M$, for $n = n_0 \ldots N$, and for $s = 1$ and 2, where $n_0 = \max(|m|, 1)$, and

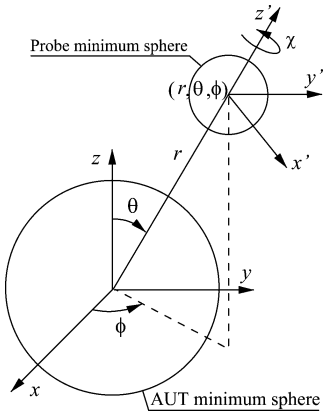

Fig. 1. The AUT and the probe minimum spheres, and the relation between the AUT and the probe coordinate systems.

M and N are the truncation numbers for the m and n indices, respectively.

The probe is assumed to be either a dual-port probe having one fixed χ orientation or a single-port probe having two χ orientations separated by 90°. The truncated SWE of the radiated electric field of one port, (p), of a reciprocal dual-port probe, $\boldsymbol{E}^{(p)}_{probe}$ is expressed as

$$\boldsymbol{E}^{(p)}_{probe}(r',\theta',\phi') = \frac{k}{\sqrt{\eta}} \sum_{\sigma\mu\nu} Q^{(p)}_{\sigma\mu\nu} \boldsymbol{F}^{(3)}_{\sigma\mu\nu}(r',\theta',\phi') \qquad (2)$$

where $Q^{(p)}_{\sigma\mu\nu}$, with $p = 1$ or 2, are the Q coefficients for the pth probe port or alternatively, in the case of a single-port probe, the pth probe orientation. The triple summation is for $\mu = -\mu_{\max} \ldots \mu_{\max}$, for $\nu = \nu_0 \ldots \nu_{\max}$, and for $\sigma = 1$ and 2, where $\nu_0 = \max(|\mu|, 1)$, and $\mu_{\max}$ and $\nu_{\max}$ are the truncation numbers for the μ and ν indices, respectively.

The truncation numbers (N, $\nu_{\max}$, M, $\mu_{\max}$) may be determined from the following truncation rules [2]:

$$N = [kr_0] + n_1 \qquad (3)$$

$$\nu_{\max} = [kr_0'] + n_1' \qquad (4)$$

$$M = [kr_C] + m_1 \qquad (5)$$

$$\mu_{\max} = [kr_C'] + m_1' \qquad (6)$$

where r_0 and r_0' are the radii of the AUT and probe minimum spheres, shown in Fig. 1, respectively, and the r_C and r_C' are the radii of the AUT and probe minimum circular cylinders [2], respectively. The square brackets indicate the largest integer smaller than or equal to the number inside the brackets. The values for the integers n_1, n_1', m_1, and m_1' are chosen according to the accuracy requirement, and typically $n_1 = n_1' = m_1 = m_1' = 10$ is sufficient [2].

C. Transmission Formula

According to the transmission formula [2], the signal at the pth probe port, $w^{(p)}$, is

$$w^{(p)}(r,\chi,\theta,\phi) = \sum_{smn} Q_{smn} \sum_{\mu=-\mu_0}^{\mu_0} P^{(p)}_{s\mu n}(kr) e^{i\mu\chi} d^n_{\mu m}(\theta) e^{im\phi} \qquad (7)$$

where $\mu_0 = \min(n, \mu_{\max})$, and $d^n_{\mu m}(\theta)$ are the rotation coefficients [2]. The probe response constants of the pth port of the probe are

$$P^{(p)}_{s\mu n}(kr) = \frac{1}{2} \sum_{\nu=\max(1,|\mu|)}^{\nu_{\max}} \sum_{\sigma=1}^{2} C^{sn(3)}_{\sigma\mu\nu}(kr) R^{(p)}_{\sigma\mu\nu} \tag{8}$$

where $C^{sn(3)}_{\sigma\mu\nu}(kr)$ are the translation coefficients of the spherical vector wave functions and $R^{(p)}_{\sigma\mu\nu}$ are the probe receiving coefficients [2].

The relations between $R^{(p)}_{\sigma\mu\nu}$, $Q^{(p)}_{\sigma\mu\nu}$ and the probe transmission coefficients $T^{(p)}_{\sigma\mu\nu}$ are [2, Eq. (5.68)],

$$R^{(p)}_{\sigma\mu\nu} = (-1)^{\mu} T^{(p)}_{\sigma-\mu\nu} \tag{9}$$

$$Q^{(p)}_{\sigma\mu\nu} = v T^{(p)}_{\sigma\mu\nu}. \tag{10}$$

Here v, with dimension $W^{1/2}$, is the normalized complex amplitude of the excitation signal at the probe port.

In the transmission formula (7) and (8), the rotation and translation coefficients are known functions, the receiving coefficients are known from a separate probe calibration measurement, and the probe port signal is known from the spherical scanning of the AUT radiated field. The formula can thus be solved for the AUT Q coefficients, and the radiated field at any larger distance, in particular, in the far field can then be obtained from (1).

III. Antenna Pattern Characterization Procedure Using a High-Order Probe

The AUT pattern characterization procedure with a high-order probe (HOP) comprises the following three steps: 1) HOP pattern calibration, 2) HOP channel balance calibration, and 3) AUT pattern measurement. In this section, these three measurements and the data processing related to each measurement are described.

A. HOP Pattern Calibration

In this calibration the HOP is treated as an AUT, and a highly linearly polarized antenna is used as an auxiliary probe. The auxiliary probe is aligned for $\chi = 0^\circ$ orientation such that its radiated field is x'-polarized in the $-z'$-axis direction. Alternatively, an additional three-antenna polarization calibration and the corresponding correction can be applied for the auxiliary probe as described in [2, Sec. 5.2.3–5.2.4].

The radiation patterns of both ports of the dual-port HOP are measured with the auxiliary probe for an appropriate number of measurement directions (θ, ϕ) for the auxiliary probe orientations $\chi = 0^\circ$ and 90°. The auxiliary probe is treated in this measurement as an electric Hertzian dipole, that is, no pattern correction is applied. This is a valid approach in the typical case where the far-field conditions hold for both the HOP and for the auxiliary probe. Hence, with the help of the well-known orthogonality integrals for the spherical vector wave functions [2], the Q coefficients of the HOP are now found from the transmission formula (7) by applying the known probe response constants of the electric Hertzian dipole. This can be done, for example, by applying the first-order probe correction technique.

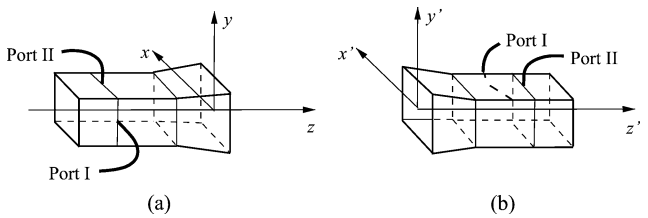

Fig. 2. (a) The probe in the AUT coordinate system $(x,\ y,\ z)$. (b) The probe in the probe coordinate system $(x',\ y',\ z')$.

During the probe pattern calibration the HOP is located in the AUT coordinate system so that the $Q^{(p)}_{smn}$ are related to the patterns of the two probe ports with the HOP pointing in the $+z$-axis direction as illustrated in Fig. 2(a). However, during the AUT pattern measurement the HOP is located in the probe coordinate system and pointed to the $-z'$-axis direction as evident from Fig. 1. According to the practice adopted at the DTU-ESA Facility, the 180° rotation of the probe is performed around the y axis as illustrated in Fig. 2. After this rotation, the coordinate system is changed from the AUT coordinate system $(x,\ y,\ z)$ to the probe coordinate system $(x',\ y',\ z')$. By the change of the indices: $s \rightarrow \sigma$, $m \rightarrow \mu$ and $n \rightarrow \nu$, the two sets of Q coefficients, $Q^{(1)}_{\sigma\mu\nu,rot}$ and $Q^{(2)}_{\sigma\mu\nu,rot}$, for the probe pointing into $-z'$-axis direction in the probe coordinate system, as illustrated in Fig. 2(b), are then obtained from [2, Eq. (5.67)],

$$Q^{(p)}_{\sigma\mu\nu,rot} = (-1)^{\nu+\mu} Q^{(p)}_{\sigma-\mu\nu}. \tag{11}$$

The $R^{(p)}_{\sigma\mu\nu}$ are determined using the relations (9) and (10) by assuming (without loss of generality), for example, $v = 1\ [W^{1/2}]$, and by replacing $Q^{(p)}_{\sigma\mu\nu} \rightarrow Q^{(p)}_{\sigma\mu\nu,rot}$ in (10). The $R^{(p)}_{\sigma\mu\nu}$ have been determined now and, thus, the probe pattern calibration has been accomplished.

It is noted that probe receiving coefficients $R^{(p)}_{\sigma\mu\nu}$ include complete information of the pattern of each port of the HOP. Thus, no separate polarization calibration, that is a part of the conventional probe calibration procedure described in [2, Sec. 5.2.3–5.2.4], is performed.

It is noted, that during the HOP pattern calibration the HOP is mounted on the flange of the AUT tower of the measurement range whereas during the AUT pattern measurement it is mounted on the flange of the probe tower. The HOP receiving coefficients must, however, remain unchanged (except for the 180° rotation of the coordinate system) in the translation of the probe. This can be ensured by suppressing the influence of mounting structure on the probe pattern by a proper application of absorbers. If, in the case of a dual-port probe, the reflection coefficient of the HOP load (once placed in the AUT tower and then in the probe tower) is different, then the HOP receiving coefficients can be ensured to remain unchanged by having a high (for example 40 dB) port-to-port isolation of the probe. In the case of poor isolation, different reflection coefficient may result in a change in the HOP pattern and thus in different probe receiving coefficients.

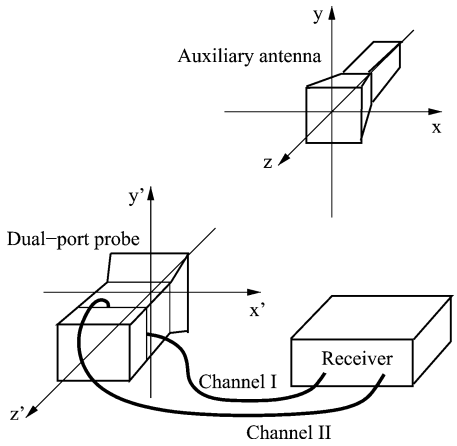

Fig. 3. Polarization scan measurement set up for determination of channel balance.

B. HOP Channel Balance Calibration

The signals measured at the receiver are influenced by not only the probe pattern but also by the two channels from the probe to the receiver; the characteristics of these two channels are generally different both in magnitude and phase. This difference must be compensated, and it is performed with the so-called the channel balance calibration measurement.

Assuming (without loss of generality) $\chi = 0°$, the transmission formula (7) for a signal at the receiver from port p can be written as

$$w_R^{(p)}(r,\theta,\phi) = c_p \sum_{smn} Q_{smn} \sum_{\mu=-\mu_0}^{\mu_0} P_{s\mu n}^{(p)}(kr) d_{\mu m}^{n}(\theta) e^{im\phi} \tag{12}$$

where c_p is the channel coefficient that is independent of any spherical mode of the probe. The c_1 and c_2 contain the information of any mismatch, attenuation, and phase propagation of the signal from the two probe ports to the receiver. The channel balance, $A_{\theta\phi}$, is defined as the ratio between the channel coefficients of the two channels,

$$A_{\theta\phi} = \frac{c_1}{c_2}, \tag{13}$$

and the purpose of the channel balance calibration is to determine this ratio. Once this ratio is known, the known received signal (12) for $p = 1$ and the known received signal (12) for $p = 2$ multiplied by $A_{\theta\phi}$ constitute the correct relative received signals.

In the channel balance calibration the HOP is located in the probe coordinate system with the fixed orientation angle $\chi = 0°$, and the auxiliary antenna is located in the AUT tower as illustrated in Fig. 3. The z axis is pointed to the origin of the probe coordinate system, thus, $\theta = 0°$. A good choice for the auxiliary antenna is an antenna with a linear polarization and the maximum radiation in the z-axis direction.

With these conditions ($\chi = 0°$, $\theta = 0°$), the signal at the receiver from the probe port p, expressed through (12), becomes

$$w_R^{(p)}(r,0,\phi) = c_p \sum_{smn} Q_{smn}^{a} P_{smn}^{(p)}(kr) e^{im\phi} \tag{14}$$

where Q_{smn}^{a} are the Q coefficients of the auxiliary antenna. The $P_{smn}^{(p)}(kr)$ are obtained from (8) using $R_{\sigma m\nu}^{(p)}$ known from the probe pattern calibration. The relation $d_{\mu m}^{n}(\theta = 0°) = \delta_{\mu m}$ [2, Eq. A2.15], where $\delta_{\mu m}$ is the Kronecker's delta, is exploited here.

The channel balance is now determined by means of the so-called polarization scan measurement where the auxiliary antenna is rotated around the z axis, and the signals from the two probe ports at the receiver are recorded in intervals of $\Delta\phi$ from $\phi = 0°$ to $360° - \Delta\phi$. The maximum $\Delta\phi$ is related to the cross-section dimensions of the probe and the auxiliary antenna in wavelengths. However, it is useful to apply a smaller $\Delta\phi$ than the maximum in this measurement for decreasing the uncertainty, because the increase in the measurement time due to this is negligible. By writing the received signal in (14) as a Fourier expansion

$$w_R^{(p)}(r,0,\phi) = \sum_{m} w_{m,R}^{(p)}(r) e^{im\phi} \tag{15}$$

with the Fourier coefficients

$$w_{m,R}^{(p)}(r) = c_p \sum_{s=1}^{2} \sum_{n=n_0}^{N} Q_{smn}^{a} P_{smn}^{(p)}(kr) \tag{16}$$

it becomes obvious that the Fourier coefficients $w_{m,R}^{(p)}(r)$ are found by the inverse discrete Fourier transformation (IDFT) of the measured signals in ϕ. The number of coefficients $w_{m,R}^{(p)}(r)$ is the same as the number of samples. However, the coefficients for $m = \pm 1$ are practically the only important coefficients here for the following reasons. First, with increasing measurement distance the coupling of the signal to the probe ports occurs increasingly dominantly via the modes with $m = \pm 1$, which is due to the asymptotic behavior of the translation coefficient [2, Eq. A3.22-A3.24]. Second, most (if not all) practical auxiliary antennas aligned on the z axis with the maximum radiation in the $+z$-axis direction possess a significant degree of power in modes with $m = \pm 1$, and this further enhances the coupling of the signal through these modes in the channel balance measurement.

Restricting the discussion now for the coefficients $m = \pm 1$ only, it is noted that depending on the polarization of the probe port, the amplitude of the coefficient $w_{m,R}^{(p)}(r)$ for $m = 1$ may differ significantly from that for $m = -1$. This is the case for highly non-linearly polarized probe port (with a linearly polarized auxiliary antenna). Due to noise and other uncertainties, the coefficient with the lower amplitude is also more sensitive to having a greater relative error than the one having the higher amplitude. For this reason, it is now suggested that for each port p the c_p is calculated for such index $m = 1$ or $m = -1$ for which the amplitude of the coefficient $w_{m,R}^{(p)}(r)$ is higher. Hence, considering now the coefficients for either $m = 1$ or $m = -1$ only, (13) and (16) provide

$$A_{\theta\phi} = \frac{w_{m',R}^{(1)}(r)}{w_{m'',R}^{(2)}(r)} \frac{\sum_{s=1}^{2} \sum_{n=1}^{N} Q_{sm''n}^{a} P_{sm''n}^{(p)}(kr)}{\sum_{s=1}^{2} \sum_{n=1}^{N} Q_{sm'n}^{a} P_{sm'n}^{(p)}(kr)}. \tag{17}$$

Here $m' = 1$ or -1 and $m'' = 1$ or -1 depending on the amplitudes of the coefficients $w^{(p)}_{m',R}(r)$ and $w^{(p)}_{m'',R}(r)$ according to above discussion.

Equation (17) allows that the probe ports are different, which is a generalization compared to the traditional first-order channel balance calibration procedure. Equation (17) requires, in general, that the auxiliary antenna Q coefficients, Q^a_{smn}, are known at least for the index m for which the c_p is determined. If a highly linearly polarized auxiliary antenna is used, then the electric Hertzian dipole assumption of the auxiliary antenna can typically be made. The Q coefficients of the electric Hertzian dipole are well known [2, Sec. 2.3.3].

It is furthermore noted that, in theory, such impractical probes may exist that do not possess radiated power in modes with $\mu = \pm 1$, and hence have a zero on-axis field. Thus, if, for some reason, such an impractical HOP were used, the channel coefficients should not be calculated from (17) for $m = -1$ or $m = 1$, but for some other value of m.

C. AUT Pattern Measurement

1) Scanning: The general high-order probe correction technique does not impose any strict requirements for the angles in θ, where the samples must be available. However, a good choice is to take the samples equidistantly in θ from 0° to 180° in steps of $\Delta\theta$ in order to ensure that the systems of linear equations, that are solved at a later stage of the probe correction calculations, have sufficient number of sufficiently linearly independent rows. It is assumed in this paper that the condition $N_\theta \geq N+2$ holds, where N_θ is the total number of sampling directions in θ from 0° to 180°. This condition follows from that for the traditional first-order probe correction technique, and although this may not be necessarily strictly required in the case the FFT/matrix inversion technique applied here, it is assumed in this paper.

For each fixed θ angle, it is required that the samples in ϕ are available from 0° to 360° $-\ \Delta\phi$ with constant increments of $\Delta\phi$. It is further required that the condition $N_\phi \geq 2M+1$ holds, where N_ϕ is the number of sampling directions in ϕ from 0° to 360° $-\ \Delta\phi$.

In each measurement direction $(\theta,\ \phi)$ received signals are measured from the two ports of the HOP, and the probe orientation angle is set to $\chi = 0°$ so that (12) becomes applicable. In the case of a single-port probe, the signals are measured for two probe orientation angles, typically for $\chi = 0°$ and 90°, in each measurement direction.

These requirements for the measurement data are conveniently fulfilled by the ϕ-scanning scheme, where stepping is made in θ and scanning in ϕ. The θ-scanning scheme, where stepping is made in ϕ and scanning in θ, is not applicable. A double ϕ-step θ-scanning scheme, and the associated high-order probe correction technique has been presented in [9].

2) Formation of the Signals at the Probe Ports: The probe correction calculations require that the correct relative received signals are known at the probe ports. Hence, the relative received signals at the two probe ports, $w^{(1)}_{rel}(r,\theta,\phi)$ and $w^{(2)}_{rel}(r,\theta,\phi)$, are formed as follows:

$$w^{(1)}_{rel}(r,\theta,\phi) = w^{(1)}_R(r,\theta,\phi) \tag{18}$$

$$w^{(2)}_{rel}(r,\theta,\phi) = A_{\theta\phi} w^{(2)}_R(r,\theta,\phi) \tag{19}$$

where $w^{(1)}_R(r,\theta,\phi)$ and $w^{(2)}_R(r,\theta,\phi)$ are the measured received signals (12) at the receiver from the two probe ports, and $A_{\theta\phi}$ is known from the channel balance calibration.

3) Probe Correction Calculations: The probe correction calculations include two steps. The first step consists of the IDFT of the signals at the probe ports. The second step consists of matrix inversions. These two steps are now explained.

In the first step, the relative received signal at the probe ports, (18) and (19) with (12), are first written as a Fourier expansion

$$w^{(p)}_{rel}(r,\theta,\phi) = \sum_{m=-M}^{M} w^{(p)}_m(r,\theta) e^{im\phi} \tag{20}$$

where

$$w^{(p)}_m(r,\theta) = \sum_{n=n_0}^{N} \sum_{s=1}^{2} Q_{smn} \sum_{\mu=-\mu_0}^{\mu_0} P^{(p)}_{s\mu n}(kr) d^n_{\mu m}(\theta) \tag{21}$$

where $n_0 = \max(1, |m|)$. The Fourier coefficients $w^{(p)}_m(r,\theta)$ for $m = -M \ldots M$ are now found for each discrete value of $\theta = 0° \ldots 180°$ for $p = 1$ and 2 by the IDFT of the measured signals in ϕ, and for the case with $N_\phi = 2M+1$ this operation can be written as

$$[w^{(p)}_m(r,\theta)|_{m=-M\ldots M}] = \mathrm{IDFT}[w^{(p)}_{rel}(r,\theta,\phi_j)|_{j=1,2\ldots N_\phi}]. \tag{22}$$

In the second step, for each fixed $m = -M \ldots M$ an overdetermined system of linear equations is set up from (21) for the unknowns Q_{smn} with indices $s = 1$ and 2, and $n = n_0 \ldots N$. For each m, this system of linear equations is written as

$$\bar{\bar{G}}_m \bar{Q}_m = \bar{W}_m. \tag{23}$$

Here, the matrix $\bar{\bar{G}}_m$ is

$$\bar{\bar{G}}_m = \begin{bmatrix} \bar{\bar{g}}^{(m)}_{11} & \cdots & \bar{\bar{g}}^{(m)}_{1N'} \\ \vdots & & \vdots \\ \bar{\bar{g}}^{(m)}_{N_\theta 1} & \cdots & \bar{\bar{g}}^{(m)}_{N_\theta N'} \end{bmatrix} \tag{24}$$

where the 2×2 block matrices $\bar{\bar{g}}^{(m)}_{ln'}$ are

$$\bar{\bar{g}}^{(m)}_{ln'} = \begin{bmatrix} g^{(1)}_{1mn}(r,\theta_l) & g^{(1)}_{2mn}(r,\theta_l) \\ g^{(2)}_{1mn}(r,\theta_l) & g^{(2)}_{2mn}(r,\theta_l) \end{bmatrix} \tag{25}$$

with

$$g^{(p)}_{smn}(r,\theta_l) = \sum_{\mu=-\mu_0}^{\mu_0} P^{(p)}_{s\mu n}(kr) d^n_{\mu m}(\theta_l). \tag{26}$$

The relation between indices n and n' is $n = n' + n_0 - 1$, and for $n' = 1 \ldots N'$ the $n = n_0 \ldots N$. The θ_l is the lth θ angle $(l = 1 \ldots N_\theta)$.

The vectors $\bar{W}_m$ and $\bar{Q}_m$ are

$$\bar{W}_m = [w^{(1)}_m(r,\theta_1), w^{(2)}_m(r,\theta_1) \ldots w^{(1)}_m(r,\theta_{N_\theta}), w^{(2)}_m(r,\theta_{N_\theta})]^{\mathrm{T}} \tag{27}$$

$$\bar{Q}_m = [Q_{1mn_0}, Q_{2mn_0} \ldots Q_{1mN}, Q_{2mN}]^{\mathrm{T}} \tag{28}$$

respectively, where $^{\mathrm{T}}$ denotes transpose.

The least-square solution to the matrix (23) is

$$\bar{Q}_m = \bar{\bar{G}}_m^{+} \bar{W}_m \tag{29}$$

where the $\bar{\bar{G}}_m^{+}$ is

$$\bar{\bar{G}}_m^{+} = (\bar{\bar{G}}_m^{\mathrm{H}} \bar{\bar{G}}_m)^{-1} \bar{\bar{G}}_m^{\mathrm{H}} \tag{30}$$

where $^{\mathrm{H}}$ denotes Hermitian transpose. The $\bar{\bar{G}}_m^{+}$ in (30) can be found from $\bar{\bar{G}}_m$ using, for example, the PINV-function in MatLAB.

Computer calculations indicate that the computational complexity of the matrix inversions is of the order of $O(N^4)$, and it is not higher for filling in the matrices. The overall computation time is dominantly determined by the time required for filling and inverting the $\bar{\bar{G}}_m$ matrices for $-N \leq m \leq N$. For example, for $N = 80$ and 160, with $M = N$, $\mu_{\max} = 7$, and $\nu_{\max} = 20$, the overall computation time is approximately 6 and 30 minutes, respectively, with the current implementation of the probe correction algorithms at the DTU-ESA Facility on a normal PC of today. In these cases, the time required for the matrix fillings was approximately 2 to 3 times the time required for the matrix inversions. It is possible to apply parallel processing for reducing the computation time.

The condition numbers of the $\bar{\bar{G}}_m$ matrices are typically the highest for $|m| = 1$. A quantitative investigation carried out in [5] with several different high-order probes shows that the condition numbers are steadily increasing with increasing N but remain below 40 with $N = 200$ for all examined probes.

The memory requirements of the technique are dominated by the size of the $\bar{\bar{G}}_m$ matrix. At a given time it is necessary to have only one $\bar{\bar{G}}_m$ matrix in memory. The $\bar{\bar{G}}_m$ matrix is the largest for the indices $|m| \leq 1$, and then its dimension is of the order of $2(N+2) \times 2N$. For example, for $N = 1000$, that corresponds to the AUT with the radius of the minimum sphere of more then 75 λ, the required memory for one $\bar{\bar{G}}_m$ matrix for any of the indices $|m| \leq 1$ in the double-precision system is of the order of 64 MB. For comparison, the maximum dimension of a single array accepted by MatLAB™ in a 32-bit Windows system is more than 600 MB.

IV. Measurements and Data Processing

This section describes the measurements carried out to validate the new antenna pattern characterization procedure based on the FFT/matrix inversion technique and to illustrate its importance for a high-order probe.

The probe in the earlier measurements, reported in [11], was a wideband dual-polarized probe SP800 from Satimo [14] covering the frequency range 0.8–3.2 GHz. Although, this SP800 probe must be, as noted in [5] and [11], considered a high-order probe, and hence cannot be treated as a first-order probe in accurate spherical near-field antenna measurements, the radiated power in the azimuthal spherical modes with $|\mu| \neq 1$ relative to the power in the modes with $|\mu| = 1$ for this probe was, however, modest. For this reason it was decided that another test measurement is carried out with a more challenging probe possessing substantial relative power in the modes with $|\mu| \neq 1$. Therefore the probe for the second test measurement reported in this paper is chosen to be an offset single-port square waveguide probe. The offset, in particular, increases the radiated power in the modes with $|\mu| \neq 1$. Since the channel balance calibration for a dual-port HOP was verified by the earlier measurements [5], [11], it is found sufficient to perform the measurements now with a single-port probe.

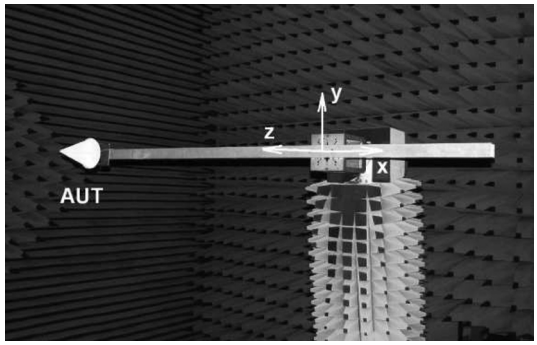

Fig. 4. Photograph of the AUT and its coordinate system.

First, the reference measurement performed for the chosen AUT is described. Next, the HOP, its characterization, and its properties in terms of the spherical wave coefficients are presented. Then, the test measurement performed for the same AUT with the HOP are described. Finally, the comparison between the reference and test AUT patterns is made, and the significance of the high-order probe correction documented.

A. Reference Measurement of the AUT

A reference full-sphere measurement is performed at the DTU-ESA Facility for the AUT illustrated in Fig. 4. The AUT is a log-periodic 1–18 GHz antenna in an offset configuration attached to a metallic support arm. The offset of the log-periodic antenna is 1.6 m from the z axis along the $-x$ axis, i.e., the coordinates of the log-periodic antenna in the AUT measurement coordinate system are (-1.6 m, 0 m, 0 m).

The choice of this AUT configuration is driven by the intention to have a demanding measurement case for which the influence of the high-order modes of the probe is expected to be large. Due to the offset, the phase of the received near-field signal varies strongly with the AUT positioning angle, and this results in a wide spectrum of spherical wave modes in the expansion of the AUT field. In addition, the non-symmetric location of the radiating element tests the sensitivity of the processing algorithm to small mechanical imperfections of the setup. Obtaining a good agreement for the chosen AUT configuration is thus expected to guarantee similar or better agreement for any other AUTs, including also large and symmetrically located AUTs, with the equal or smaller radius of the AUT minimum sphere.

The reference measurement of the AUT is carried out for the x-polarized port of the AUT at 1.4 GHz and 1.5 GHz. The scanning scheme is chosen to be scanning in θ within $0^\circ \leq \theta < 360^\circ$ and stepping in ϕ within $0^\circ \leq \phi < 180^\circ$ with sampling intervals $\Delta\theta = \Delta\phi = 2.4^\circ$. This reference measurement is performed with a high-quality dual-polarized open-ended choked circular waveguide probe, that is a first-order probe.

In the data processing, the traditional first-order probe correction is applied to the received probe signals and the far field is

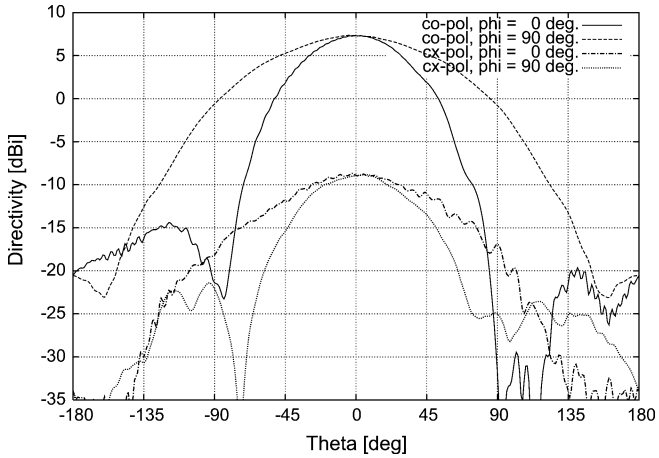

Fig. 5. Reference AUT pattern: co-polar directivity for $\phi = 0^\circ$ (solid) and $\phi = 90^\circ$ (dashed) planes and cross-polar directivity for $\phi = 0^\circ$ (dash-doted) and $\phi = 90^\circ$ (dotted) planes.

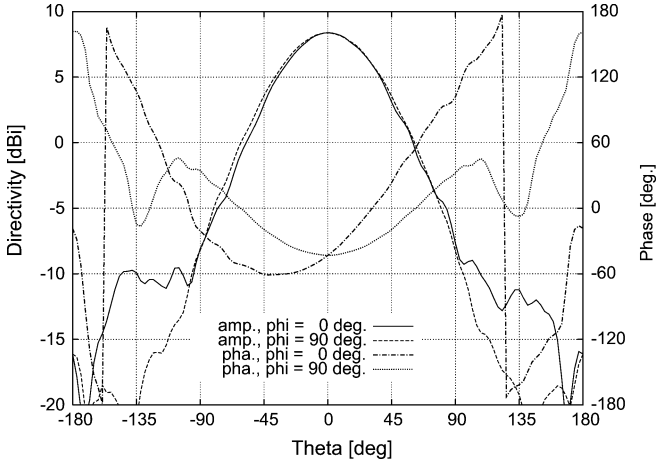

Fig. 6. Measured pattern of the offset square waveguide probe (HOP): co-polar directivity for the $\phi = 0^\circ$ (solid) and $\phi = 90^\circ$ (dashed) planes and co-polar phase for the $\phi = 0^\circ$ (dash-doted) and $\phi = 90^\circ$ (dotted) planes.

calculated. This far field is considered as a reference in the comparisons below. The 1-σ uncertainty of the reference pattern is estimated to be lower than 0.05 dB around the pattern peak.

The co-polar and cross-polar directivities of the AUT reference pattern at 1.5 GHz, calculated according to the Ludwig's third definition [15], are shown for the $\phi = 0^\circ$ and $\phi = 90^\circ$ planes in Fig. 5. The small ripples at low levels of the co-polar pattern in the $\phi = 0^\circ$ plane are due to the interference of the direct field from the radiating log-periodic element of the AUT and the diffracted field from the opposite end of the metallic support arm of the AUT.

B. HOP Pattern Calibration

As stated earlier the HOP is an open-ended square waveguide with the center of the aperture offset from the center of the probe coordinate system. This offset is 30.5 mm along the $+x'$ axis. This corresponds to about 0.15 wavelengths at 1.5 GHz.

The HOP pattern calibration is performed using a calibrated first-order probe as the auxiliary probe. The auxiliary probe is the same probe that was used for the reference AUT measurement. Since the chosen HOP is a single-port antenna, only one pattern measurement is required. During the HOP pattern calibration the HOP is placed in the AUT coordinate system so that its radiation is x-polarized in the z-axis direction. The pattern of the HOP oriented for the y polarization is found by applying a 90° rotation of the obtained HOP pattern around the z axis. The probe receiving coefficients for the two polarizations, $R^{(1)}_{\sigma\mu\nu}$ and $R^{(2)}_{\sigma\mu\nu}$, are finally determined according to Section III-A.

The co-polar amplitude and phase patterns of the HOP at 1.5 GHz are shown in Fig. 6. It is seen that the amplitude pattern is almost symmetric with a small asymmetry in the $\phi = 0^\circ$ plane. On the other hand, the phase pattern is clearly asymmetric in the $\phi = 0^\circ$ plane due to the offset of the probe.

The normalized spherical μ-mode power spectrum of the HOP is then calculated from the determined probe receiving coefficients. This spectrum, that describes the relative power of the field radiated by the probe as a function of the azimuthal mode index $|\mu| = 0 \ldots M$, is shown in Fig. 7. For completeness, the normalized spherical ν-mode power spectrum of the HOP and the normalized spherical μ-mode power spectrum of the first-order probe are also presented in Fig. 7.

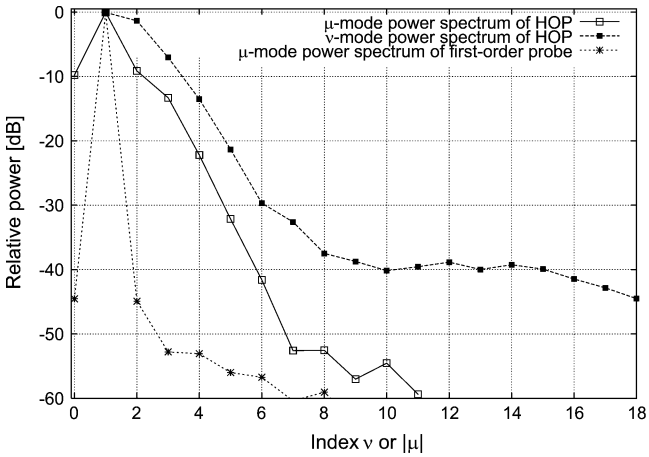

Fig. 7. The normalized spherical μ-mode and ν-mode power spectra of the offset square waveguide probe, and the normalized spherical μ-mode power spectrum of the first-order probe used in the reference AUT measurement.

It is seen from the μ-mode spectrum of the HOP that, though most of its radiated power is contained in the modes with $|\mu| = 1$, a significant part of the power is contained also in the other modes. In particular, the power in the modes with $|\mu| = 0$, 2, and 3, as compared to the $|\mu| = 1$ modes, is in the range from -10 dB to -13 dB. Thus, the presented spectrum of the HOP clearly illustrates that the offset square waveguide probe is indeed a high-order probe. For comparison, in the case of the first-order probe, as seen in Fig. 7, practically all the power is concentrated in the modes with $|\mu| = 1$.

C. Test Measurement of the AUT and Data Processing

In line with the requirements to the scanning described in Section III-C, a full-sphere near-field measurement with the HOP is performed for the AUT using the ϕ-scanning scheme with two HOP polarizations. The sampling intervals in ϕ and θ are chosen to be $\Delta\phi = 2.4^\circ$ and $\Delta\theta = 2.4^\circ$, respectively, as in the reference measurement.

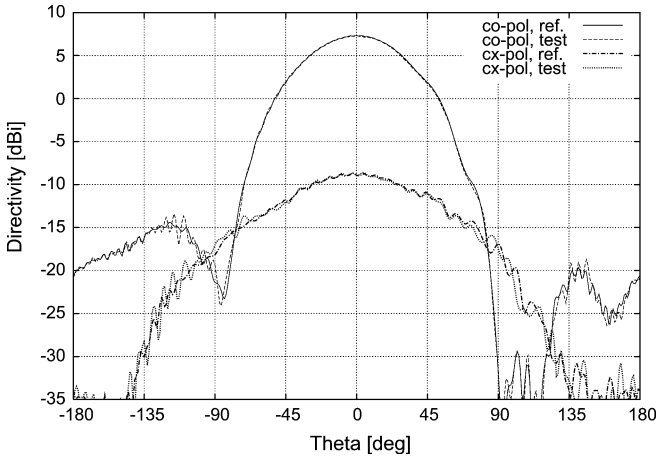

Fig. 8. Comparison between the reference and test AUT patterns in $\phi = 0^\circ$ plane: reference (solid) and test (dashed) co-polar directivity, and reference (dash-doted) and test (dotted) cross-polar directivity.

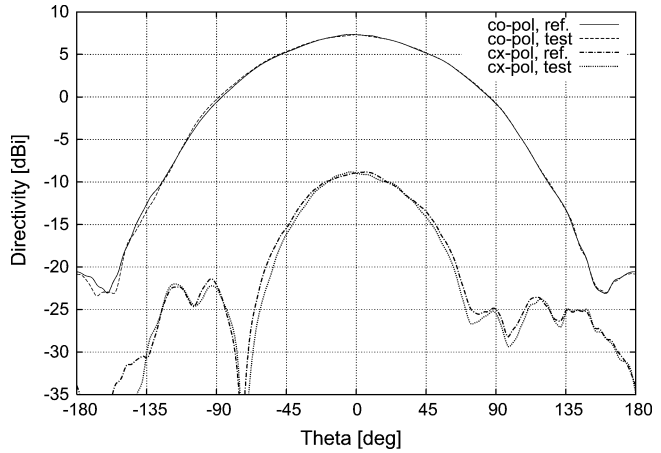

Fig. 9. Comparison between the reference and test AUT patterns in $\phi = 90^\circ$ plane: reference (solid) and test (dashed) co-polar directivity, and reference (dash-doted) and test (dotted) cross-polar directivity.

For the calculation of the Q coefficients of the AUT field, and subsequently the far field from (1), the measured probe signals are processed according to the procedure described in Section III-C. The μ and ν modes of the probe up to $\mu_{\max} = 6$ and $\nu_{\max} = 8$, respectively, are taken into account. The truncation numbers for the probe modes are selected on the condition that only the modes above the noise floor are included in the calculations. The probe response constants are obtained from (8) using the probe receiving coefficients known from the probe pattern calibration. The channel balance is set to 1.

The obtained reference and test directivity patterns of the AUT for 1.5 GHz are shown for the $\phi = 0^\circ$ plane in Fig. 8 and for the $\phi = 90^\circ$ plane in Fig. 9. It is seen from Figs. 8 and 9 that there is a good agreement between the co-polar patterns in both planes though the test pattern shows slightly larger ripples around $\theta = \pm 120^\circ$ in the $\phi = 0^\circ$ plane. Agreement between the cross-polar patterns is also good, though some small differences can be observed.

The statistics for the difference between the reference and test co-polar AUT patterns in the dB scale calculated for the region $|\theta| \leq 10^\circ$, i.e., around the pattern peak, are given in Table I.

TABLE I
STATISTICAL DATA FOR THE DIFFERENCE BETWEEN THE REFERENCE AND TEST CO-POLAR AUT PATTERNS WITHIN $|\theta| \leq 10^\circ$

	Co-polar directivity [dB]		Co-polar phase [°]	
f [GHz]	Mean	Std.	Mean	Std.
1.4	0.026	0.044	0.28	0.88
1.5	0.048	0.050	0.13	1.16

TABLE II
STATISTICAL DATA FOR THE DIFFERENCE BETWEEN THE REFERENCE AND TEST ($M = 1$ AND $N = 8$) CO-POLAR PATTERNS WITHIN $|\theta| \leq 10^\circ$

	Co-polar directivity [dB]		Co-polar phase [°]	
f [GHz]	Mean	Std.	Mean	Std.
1.4	0.213	0.229	5.31	2.24
1.5	0.266	0.305	6.67	2.69

The mean and the standard deviation of the difference between the test and reference patterns do not exceed 0.05 dB. The observed deviations for the co-polar directivity are within the measurement uncertainty for the standard measurement procedure at the DTU-ESA Facility employing the first-order probes and the first-order probe correction technique, and the agreement is thus considered to be very good. Similar agreement between the co-polar directivities was observed also in the final measurement in [5]. The deviations for the co-polar phase seen in Table I are larger than it was observed in [5], but in view of the challenging AUT and the HOP, these values are found acceptable.

The test data are also processed taking into account only $|\mu| \leq 1$ modes of the HOP to study the influence of the high-order azimuthal modes on the accuracy of the obtained far-field data. The statistics for the difference between the reference co-polar pattern and test co-polar pattern processed with $\mu_{\max} = 1$ and $\nu_{\max} = 8$ calculated for the same region $|\theta| \leq 10^\circ$ are given in Table II. The statistics show that in this case the difference between the test and reference patterns is several times larger as compared to the results in Table I. This was expected, and it confirms the fact that the proper high-order probe correction is clearly necessary for the employed HOP.

V. CONCLUSION

A complete antenna pattern characterization procedure for probe-corrected spherical near-field antenna measurements with high-order probes has been developed and described in this paper. The procedure has been verified by measurements in the DTU-ESA Spherical Near-Field Antenna Test Facility. The uncertainty of the antenna pattern determination provided by the new procedure with a high-order probe is comparable to that provided by the existing procedure based on the use of first-order probes.

The results of this paper have shown that accurate antenna pattern characterization using high-order probes is possible both in theory and practice using the ϕ-scanning scheme. Future work could include similar thorough theoretical and practical investigations of the possibilities for accurate antenna pattern characterization with high-order probes with other scanning schemes, for example, with the θ-scanning scheme.

ACKNOWLEDGMENT

The authors would like to thank J. Lemanczyk from ESTEC for valuable comments and suggestions.

REFERENCES

[1] DTU-ESA Spherical Near-Field Antenna Test Facility Technical University of Denmark [Online]. Available: http://www.dtu.dk/centre/ems/English/research/facilities.aspx

[2] J. E. Hansen, *Spherical Near-Field Antenna Measurements*. London, U.K.: Peter Peregrinus, 1988.

[3] T. A. Laitinen, S. Pivnenko, and O. Breinbjerg, "Odd-order probe correction technique for spherical near-field antenna measurements," *Radio Sci.*, vol. 40, no. 5, 2005.

[4] T. A. Laitinen, S. Pivnenko, and O. Breinbjerg, "Iterative probe correction technique for spherical near-field antenna measurements," *IEEE Antennas Wireless Propag. Lett.*, vol. 4, 2005.

[5] T. A. Laitinen, S. Pivnenko, J. Nielsen, and O. Breinbjerg, "Development of 1–3 GHz Probes for the DTU-ESA Spherical Near-Field Antenna Test Facility. ESTEC Contract/04/NL/LvH/bj. Final Report, Volume 1: Executive Summary," Electromagnetic Systems, Ørsted·DTU, Tech. Univ. Denmark, Lyngby, Denmark, 2006, Rep. R 729.

[6] T. A. Laitinen and S. Pivnenko, "Probe correction technique for symmetric odd-order probes for spherical near-field antenna measurements," *IEEE Antennas Wireless Propag. Lett.*, vol. 6, 2007.

[7] C. H. Schmidt, M. M. Leibfritz, and T. F. Eibert, "Fully probe-corrected near-field to far-field transformation employing plane wave expansion and diagonal translation operators," *IEEE Trans. Antennas Propag.*, vol. 56, pp. 737–746, Mar. 2008.

[8] T. A. Laitinen and O. Breinbjerg, "A first/third-order probe correction technique for spherical near-field antenna measurements using three probe orientations," *IEEE Trans. Antennas Propag.*, vol. 56, pp. 1259–1268, May 2008.

[9] T. A. Laitinen, "Double ϕ-step θ -scanning technique for spherical near-field antenna measurements," *IEEE Trans. Antennas Propag.*, vol. 56, pp. 1633–1639, Jun. 2008.

[10] C. H. Schmidt and T. F. Eibert, "Multilevel plane wave based near-field far-field transformation for electrically large antennas in free-space and above material halfspace," *IEEE Trans. Antennas Propag.*, vol. 57, pp. 1382–1390, May 2009.

[11] T. Laitinen, J. M. Nielsen, S. Pivnenko, and O. Breinbjerg, "On the application range of general high-order probe correction technique in spherical near-field antenna measurements," presented at the 2nd Eur. Conf. on Antennas and Propagation (EuCAP'07), Edinburgh, U.K., Nov. 2007.

[12] T. A. Laitinen, S. Pivnenko, and O. Breinbjerg, "Sensitivities of various probe correction techniques to noise and inaccurate channel balance in spherical near-field antenna measurements," in *Proc. 2nd Int. Conf. on Electromagnetic Near-Field Characterization and Imaging (Iconic'05)*, Barcelona, Spain, 2005, pp. 411–416.

[13] *IEEE Standard Test Procedures for Antennas*, IEEE Std 149-1979, 1979.

[14] Satimo [Online]. Available: http://www.satimo.org

[15] A. C. Ludwig, "The definition of cross polarization," *IEEE Trans. Antennas Propag.*, vol. 21, pp. 116–119, Jan. 1973.

Tommi Laitinen (M'09) was born in Pihtipudas, Finland, on March 19, 1972. He received the Master of Science in Technology, the Licentiate of Science in Technology, and the Doctor of Science in Technology degrees in electrical engineering from Helsinki University of Technology (TKK), Espoo, Finland, in 1998, 2000, and 2005, respectively.

He joined the Radio Laboratory at TKK as a Master's thesis student in 1997, and continued as a doctoral student in the same place afterwards. His major research interests at TKK were small antenna measurements. From 2003 until the end of 2006, he was with the Technical University of Denmark (DTU) as a Postdoctoral Researcher and Assistant Professor. His research interests at DTU were spherical near-field antenna measurements. During these years, he mainly contributed to the development of an accurate antenna pattern characterization procedure for the DTU-ESA Spherical Near-Field Antenna Test Facility based on spherical near-field antenna measurements with a high-order probe. In the beginning of 2007 until the end of 2009, he was with the Radio Laboratory at TKK. In the beginning of 2010, he joined the Department of Radio Science and Engineering, Aalto University, Aalto, Finland, as a Senior Researcher. While still carrying on with research on spherical near-field antenna measurements, he now works also with small antenna measurements and sensor applications. His other duties include occasionally teaching master's and postgraduate courses at Aalto University. He is the author or coauthor of approximately 50 journal and conference papers.

Dr. Laitinen is the recipient of the IEEE Antennas and Propagation Society's 2009 R. W. P. King Award for one of his papers.

Sergey Pivnenko (M'98) was born in Kharkiv, Ukraine, in 1973. He received the M.Sc. and Ph.D. degrees in electrical engineering from Kharkiv National University, Ukraine, in 1995 and 1999, respectively.

From 1998 to 2000, he was a Research Fellow at the Radiophysics Department, Kharkiv National University. In 2000, he joined the Antennas and Electromagnetics Group, Department of Electrical Engineering, Technical University of Denmark, where he now works as an Associate Professor and operates the DTU-ESA Spherical Near-Field Antenna Test Facility. Since 2000, he participated to several research projects related to design, development and characterization of satellite antennas, development of new near-field probes and probe correction techniques for near-field antenna measurements. From 2004–2007, he was a work package leader in the European Union network "Antenna Center of Excellence" where he was responsible for antenna measurement facility comparisons and participated to the other activities related to antenna measurements. He is the author or coauthor of more than 70 journal and conference papers. His research interests include antenna measurement techniques, antenna analysis and design.

Jeppe Majlund Nielsen was born on June 9, 1976. He received the M.Sc. degree in engineering from the Technical University of Denmark (DTU), Kgs. Lyngby, in 2002.

Since then he has been a Research Assistant in the Department of Electrical Engineering, DTU. His work has included antenna gain calibrations by spherical near-field antenna measurements as well as planar near-field antenna measurements. He has supervised several M.Sc. projects, M.Sc. courses and special courses on antenna theory and measurements. He has participated in projects related to high-order probe correction for spherical near-field antenna measurements. He is a coauthor of nine conference papers.

Olav Breinbjerg (M'87) was born in Silkeborg, Denmark, on July 16, 1961. He received the M.Sc. and Ph.D. degrees in electrical engineering from the Technical University of Denmark (DTU), Kgs. Lyngby, in 1987 and 1992, respectively.

Since 1991 he has been on the faculty of the Department of Electrical Engineering, DTU (formerly Ørsted·DTU, Department of Electromagnetic Systems, and Electromagnetics Institute) where he is now a Full Professor and Head of the Electromagnetic Systems Group including the DTU-ESA Spherical Near-Field Antenna Test Facility. He was a Visiting Scientist at Rome Laboratory, Hanscom Air Force Base, Massachusetts, in fall 1988 and a Fulbright Research Scholar at the University of Texas at Austin, in spring 1995. His research is generally in applied electromagnetics—and particularly in antennas, antenna measurements, computational techniques and scattering—for applications in wireless communication and sensing technologies. At present, his interests focus on metamaterials, antenna miniaturization, and spherical near-field antenna measurements. He is the author or coauthor of more than 40 journal papers, 100 conference papers, and 70 technical reports, and he has been, or is, the main supervisor of 10 Ph.D. projects. He has taught several B.Sc. and M.Sc. courses in the area of applied electromagnetic field theory on topics such as fundamental electromagnetics, analytical and computational electromagnetics, antennas, and antenna measurements at DTU, where he has also supervised more than 70 special courses and 30 M. Sc. final projects. Furthermore, he has given short courses at other European universities. He is currently the coordinating teacher at DTU for the 3rd semester course 31400 Electromagnetics, and the 7–9th semester courses 31428 Advanced Electromagnetics, 31430 Antennas, and 31435 Antenna Measurements in Radio Anechoic Chambers.

Prof. Breinbjerg received a US Fulbright Research Award in 1995, the 2001 AEG Elektron Foundation's Award in recognition of his research in applied electromagnetics, and the 2003 DTU Student Union's Teacher of the Year Award for his course on electromagnetics.